Dynamical mean-field theory for strongly correlated inhomogeneous multilayered nanostructures

J. K. Freericks*
Department of Physics, Georgetown University, Washington, DC 20057, USA
(Received 10 August 2004; published 29 November 2004)

Dynamical mean field theory is employed to calculate the properties of multilayered inhomogeneous devices composed of semi-infinite metallic lead layers coupled via barrier planes that are made from a strongly correlated material (and can be tuned through the metal-insulator Mott transition). We find that the Friedel oscillations in the metallic leads are immediately frozen in and do not change as the thickness of the barrier increases from one to 80 planes. We also identify a generalization of the Thouless energy that describes the crossover from tunneling to incoherent ohmic transport in the insulating barrier. We qualitatively compare the results of these self-consistent many-body calculations with the assumptions of non-self-consistent Landauer-based approaches to shed light on when such approaches are likely to yield good results for the transport.

DOI: 10.1103/PhysRevB.70.195342 PACS number(s): 71.30.+h, 73.40.Rw, 73.20.−r, 73.40.−c

I. INTRODUCTION

The fields of strongly correlated materials and of nanotechnology are being united by work that investigates what happens when correlated materials are placed into inhomogeneous environments on the nanoscale. This can be accomplished by careful growth of strongly correlated materials with molecular beam epitaxy or pulsed laser deposition, or it may be an intrinsic property of some strongly correlated systems that display either nanoscale phase separation, or nanoscale inhomogeneity. There are fundamental questions about these systems—what happens to the properties of the system when it has inhomogeneities on the nanoscale and how does this spatial confinement modify the quantum-mechanical correlations?

We investigate a special case of a correlated nanostructure, where we can carefully control the quantum confinement effects. We take a semi-infinite ballistic-metal lead and couple it to another semi-infinite ballistic-metal lead via a strongly correlated barrier material (which is from one to 80 atomic planes thick). As the barrier is made thinner, the strongly correlated system is being confined in one spatial direction between the metallic leads. But the metallic leads induce a proximity effect on the barrier, which can deconfine the correlated system. Indeed, we will see that systems with a single-plane barrier still display upper and lower Mott bands, but they also have a low-energy low-weight peak to the density of states that arises from the proximity-effect induced states that are localized near the interfaces of the leads and the barrier. As the barrier is made thicker, this peak becomes a dip, which decreases exponentially with the thickness.

We employ dynamical mean field theory (DMFT) in this work. This allows us to self-consistently calculate the properties of the inhomogeneous system, including Friedel-type oscillations in the leads, and the proximity-effect on the barrier. We do not need to make any assumptions about the kind of transport through this device, be it ballistic, diffusive, tunneling, or incoherent (via thermal excitations), since the DMFT automatically incorporates all kinds of transport within its formalism.[1] We are, however, making one approximation in this approach—namely, we make the assumption that the self-energy remains local, even though it can vary from plane to plane in the multilayered nanostructure. Such an approximation should work fine for these inhomogeneous systems, since the coordination number remains the same throughout the device (and we are working in three dimensions). This is to be contrasted with more conventional approaches to tunneling, which assume a single-particle approach and employ a phenomenological potential to describe the barrier region.[2] The wave functions, transmission, and reflection coefficients can be calculated, and then the transport analyzed, as in a Landauer-based approach. In the DMFT calculations, we determine the potential self-consistently (i.e., the self-energy) from the microscopic parameters of the Hamiltonian, and the potential can vary with the energy of the scattering states. It is not clear that a simple phenomenological potential can reproduce the same kind of behavior via a conventional tunneling approach.

We assume each of the multilayer planes has translational invariance in the perpendicular x and y directions. This allows us to use a mixed basis, Fourier transforming the two perpendicular directions to k_x and k_y, but keeping the z direction in real space. Then for each two-dimensional band energy, we have a quasi-one-dimensional problem to solve, which has a tridiagonal representation in real space, and can be solved with a renormalized perturbation expansion.[3] It is this mixed-basis representation (introduced by Potthoff and Nolting[1]) that allows us to solve this problem. By iterating our many-body equations, we can achieve a self-consistent solution.

In addition to single-particle properties, we also evaluate z-axis transport, perpendicular to the multilayers. Thouless introduce the idea of using the dwell time within the barrier to define a quantum energy scale $\hbar/t_{\mathrm{dwell}}$, which turned out to describe the dynamics and transport of both ballistic metal and diffusive metal barriers.[4,5] The concept has been applied widely to the quasiclassical theory of Josephson junctions as well.[6] If we do not focus on the time spent within the barrier, but instead try to extract an energy scale from the resistance of a device, then we can generalize the Thouless energy to

the case of an insulating barrier, where the transport arises from either tunneling or incoherent (thermally activated) processes. We find that when this energy scale is on the order of the temperature, then we have a crossover from tunneling to incoherent transport. A short communication of this work has already appeared.[7]

The organization of this paper is as follows: in Sec. II, we present a detailed derivation of the formalism and the numerical algorithms used to calculate properties of nanostructures. In Sec. III, we describe the single-particle properties, focusing on the density of states and the self-energy. In Sec. IV, we generalize the concept of the Thouless energy, which is applied to charge transport in Sec. V. We end with our conclusions in Sec. VI.

II. FORMALISM AND NUMERICAL ALGORITHMS

The Hamiltonian we consider involves a hopping term for the electrons and an interaction term for the sites within the barrier region (interactions can be added in the metal if desired to convert the leads from a ballistic metal to a diffusive metal, but we do not do so here). For the interaction, we employ the Falicov-Kimball model[8] which involves an interaction between the conduction electrons with localized particles (thought of as *f*-electrons or charged ions) when the conduction electron hops onto a site occupied by the localized particle. The Falicov-Kimball model has a non-Fermi liquid ground state in the metallic regime, because the electrons see static charge scatterers, which always produce a finite lifetime, so it has no quasiparticle resonance associated with it, as seen in other strongly correlated models like the Hubbard and periodic Anderson model. It also has a Mott-type metal-insulator transition, that sets in when the correlation strength is large enough. Our choice of using the Falicov-Kimball model is pragmatic, since the DMFT can be easily solved for this system. We expect the results in the insulating phase to resemble other correlated insulators, since the most important property of an insulator is the size of its gap. On the metallic side, the Falicov-Kimball model is good for describing the crossover from ballistic to diffusive transport in dirty metals, but it is unable to describe the coherent quasiparticle formation, with a renormalized Fermi energy seen in pure systems. We feel it is nevertheless an interesting model to consider for examining systems near a Mott transition. We consider spinless electrons here, but spin can be included trivially by introducing a factor of 2 into some of the results. The Hamiltonian is

$$\mathcal{H} = -\sum_{ij} t_{ij} c_i^\dagger c_j + \sum_i U_i \left(c_i^\dagger c_i - \frac{1}{2} \right) \left(w_i - \frac{1}{2} \right), \tag{1}$$

where t_{ij} is a Hermitian hopping matrix, U_i is the Falicov-Kimball interaction, and w_i is a classical variable that equals one if there is a localized particle at site i and zero if there is no localized particle at site i (a chemical potential μ is employed to adjust the conduction-electron concentration). Since we are considering multilayered heterostructures, we assume that the hopping matrix is translationally invariant within each plane, as well as the Falicov-Kimball interaction. We let the z direction denote the direction where the system is allowed to have inhomogeneity. Then our translational invariance in the parameters requires that $U_i = U_j$ if $\mathbf{R}_i - \mathbf{R}_j$ has a vanishing z component. Similarly, $t_{ij} = t_{i'j'}$ if $\mathbf{R}_i - \mathbf{R}_{i'}$ and $\mathbf{R}_j - \mathbf{R}_{j'}$ both have a vanishing z component, and $\mathbf{R}_i - \mathbf{R}_j = \mathbf{R}_{i'} - \mathbf{R}_{j'}$. But this requirement is quite modest, and allows for many complex situations to be considered.

We denote the planes with a given z component by a greek label $(\alpha, \beta, \gamma, \ldots)$. Then our requirement on the interaction is that U_α has a definite value for each plane α. The hopping matrix can have one value $t_\alpha^\parallel$ for the hopping within the plane, and different values $t_{\alpha,\alpha+1}$ and $t_{\alpha-1,\alpha}$ for hopping to the plane to the right and for hopping to the plane to the left, respectively. For simplicity, we will only consider nearest-neighbor hopping here, and we assume the lattice positions $\mathbf{R}_i$ all lie on the points of a simple cubic lattice (but we do not have full cubic symmetry).

Because of the translational invariance within each plane, we can perform a Fourier transform in the x and y coordinates to the mixed basis $\mathbf{k}_x$, $\mathbf{k}_y$, and α (the z component in real space). We define the two-dimensional band structure, for each plane α, by

$$\epsilon_\alpha^{2d}(\mathbf{k}_x, \mathbf{k}_y) = -2t_\alpha^\parallel [\cos \mathbf{k}_x + \cos \mathbf{k}_y]. \tag{2}$$

The Green's function, in real space, is defined by

$$G_{ij}(\tau) = -\langle \mathcal{T}_\tau c_i(\tau) c_j^\dagger(0) \rangle, \tag{3}$$

for imaginary time τ. The notation $\langle \mathcal{O} \rangle$ denotes the trace $\mathrm{Tr} \exp(-\beta[\mathcal{H} - \mu\mathcal{N}])\mathcal{O}$ divided by the partition function $\mathcal{Z} = \mathrm{Tr} \exp(-\beta[\mathcal{H} - \mu\mathcal{N}])$ and the operators are expressed in the Heisenberg representation $\mathcal{O}(\tau) = \exp(\tau[\mathcal{H} - \mu\mathcal{N}])\mathcal{O} \times \exp(-\tau[\mathcal{H} - \mu\mathcal{N}])$. The symbol $\mathcal{T}_\tau$ denotes time ordering of operators, with earlier τ values appearing to the right and β is the inverse temperature ($\beta = 1/T$). We will work with the Matsubara frequency Green's functions, defined for imaginary frequencies $i\omega_n = i\pi T(2n+1)$. The Green's function at each Matsubara frequency is determined by a Fourier transformation

$$G_{ij}(i\omega_n) = \int_0^\beta d\tau \, e^{i\omega_n \tau} G_{ij}(\tau). \tag{4}$$

We also will work with the analytic continuation of the time-ordered Green's functions to the real axis (retarded or advanced Green's functions), with $i\omega_n \to \omega \pm i0^+$. We use the symbol Z to denote a general variable in the complex plane (although we will mainly be interested in either $Z = i\omega_n$ or $Z = \omega + i0^+$). Finally, we work in the mixed basis described above, where we Fourier transform the x and y components to momentum space, to give $G_{\alpha\beta}(\mathbf{k}, Z)$, where $\mathbf{R}_i$ has a z component equal to α and $\mathbf{R}_j$ has a z component equal to β ($\mathbf{k}$ is a two-dimensional wave vector).

With all of this notation worked out, we can write the equation of motion for the Green's function in real space,[1] which satisfies

$$G_{ij}^{-1}(Z) = (Z+\mu)\delta_{ij} - \Sigma_i(Z)\delta_{ij} + t_{ij}. \tag{5}$$

Now we go to a mixed basis, by Fourier transforming in the x and y directions to find

$$G_{\alpha\beta}^{-1}(\mathbf{k},Z) = [Z+\mu-\Sigma_\alpha(Z)-\epsilon^{2d}(\mathbf{k})]\delta_{\alpha\beta} + t_{\alpha\alpha+1}\delta_{\alpha+1\beta} + t_{\alpha\alpha-1}\delta_{\alpha-1\beta}, \tag{6}$$

with $\Sigma_\alpha(Z)$ the local self-energy for plane α. Finally, we use the identity $\Sigma_\gamma G_{\alpha\gamma}(Z)G_{\gamma\beta}^{-1}(Z)=\delta_{\alpha\beta}$ to get the starting point for the recursive solution to the problem,

$$\delta_{\alpha\beta} = G_{\alpha\beta}(\mathbf{k},Z)[Z+\mu-\Sigma_\beta(Z)-\epsilon_\beta^{2d}(\mathbf{k})] + G_{\alpha\beta-1}(\mathbf{k},Z)t_{\beta-1\beta} + G_{\alpha\beta+1}(\mathbf{k},Z)t_{\beta+1\beta}. \tag{7}$$

The equation of motion in Eq. (7) has a tridiagonal form with respect to the spatial component z, and hence it can be solved by employing the renormalized perturbation expansion.[3] We illustrate the solution exactly here. The equation with $\beta=\alpha$ is different from the equations with $\beta\neq\alpha$. The former is solved directly via

$$G_{\alpha\alpha}(\mathbf{k},Z) = \frac{1}{Z+\mu-\Sigma_\alpha(Z)-\epsilon_\alpha^{2d}(\mathbf{k}) + \dfrac{G_{\alpha\alpha-1}(\mathbf{k},Z)}{G_{\alpha\alpha}(\mathbf{k},Z)}t_{\alpha-1\alpha} + \dfrac{G_{\alpha\alpha+1}(\mathbf{k},Z)}{G_{\alpha\alpha}(\mathbf{k},Z)}t_{\alpha+1\alpha}}, \tag{8}$$

and the latter equations can all be set into the form

$$-\frac{G_{\alpha\alpha-n+1}(\mathbf{k},Z)t_{\alpha-n+1\alpha-n}}{G_{\alpha\alpha-n}(\mathbf{k},Z)} = Z+\mu-\Sigma_{\alpha-n}(Z)-\epsilon_{\alpha-n}^{2d}(\mathbf{k}) + \frac{G_{\alpha\alpha-n-1}(\mathbf{k},Z)t_{\alpha-n-1\alpha-n}}{G_{\alpha\alpha-n}(\mathbf{k},Z)}, \tag{9}$$

for $n>0$, with a similar result for the recurrence to the right. We define the left function

$$L_{\alpha-n}(\mathbf{k},Z) = -\frac{G_{\alpha\alpha-n+1}(\mathbf{k},Z)t_{\alpha-n+1\alpha-n}}{G_{\alpha\alpha-n}(\mathbf{k},Z)} \tag{10}$$

and then determine the recurrence relation from Eq. (9),

$$L_{\alpha-n}(\mathbf{k},Z) = Z+\mu-\Sigma_{\alpha-n}(Z)-\epsilon_{\alpha-n}^{2d}(\mathbf{k}) - \frac{t_{\alpha-n\alpha-n-1}t_{\alpha-n-1\alpha-n}}{L_{\alpha-n-1}(\mathbf{k},Z)}. \tag{11}$$

We solve the recurrence relation by starting with the result for $L_{-\infty}$, and then iterating Eq. (11) up to $n=1$. Of course we do not actually go out infinitely far in our calculations. We assume we have semi-infinite metallic leads, hence we can determine $L_{-\infty}$ by substituting $L_{-\infty}$ into both the left- and right-hand sides of Eq. (11), which produces a quadratic equation for $L_{-\infty}$ that is solved by

$$L_{-\infty}(\mathbf{k},Z) = \frac{Z+\mu-\Sigma_{-\infty}(Z)-\epsilon_{-\infty}^{2d}(\mathbf{k})}{2} \pm \frac{1}{2}\sqrt{[Z+\mu-\Sigma_{-\infty}(Z)-\epsilon_{-\infty}^{2d}(\mathbf{k})]^2-4t_{-\infty}^2}. \tag{12}$$

The sign in Eq. (12) is chosen to yield an imaginary part less than zero for Z lying in the upper half plane, and vice versa for Z lying in the lower half plane. If $L_{-\infty}$ is real, then we choose the root whose magnitude is larger than $t_{-\infty}$ (the product of the roots equals $t_{-\infty}^2$). In our calculations, we assume that the left function is equal to the value $L_{-\infty}$ found in the bulk, until we are within 30 planes of the first interface [for a ballistic-metal lead $\Sigma_{-\infty}(Z)=0$]. Then we allow those 30 planes to be self-consistently determined with L_α possibly changing, and we include a similar 30 planes on the right-hand side of the last interface, terminating with the bulk result to the right as well.

In a similar fashion, we define a right function and a recurrence relation to the right, with the right function

$$R_{\alpha+n}(\mathbf{k},Z) = -\frac{G_{\alpha\alpha+n-1}(\mathbf{k},Z)t_{\alpha+n-1\alpha+n}}{G_{\alpha\alpha+n}(\mathbf{k},Z)} \tag{13}$$

and the recurrence relation

$$R_{\alpha+n}(\mathbf{k},Z) = Z+\mu-\Sigma_{\alpha+n}(Z)-\epsilon_{\alpha+n}^{2d}(\mathbf{k}) - \frac{t_{\alpha+n\alpha+n+1}t_{\alpha+n+1\alpha+n}}{R_{\alpha+n+1}(\mathbf{k},Z)}. \tag{14}$$

We solve the right recurrence relation by starting with the result for R_∞, and then iterating Eq. (14) up to $n=1$. As before, we determine R_∞ by substituting R_∞ into both the left- and right-hand sides of Eq. (14), which produces a quadratic equation for R_∞ that is solved by

$$R_\infty(\mathbf{k},Z) = \frac{Z+\mu-\Sigma_\infty(Z)-\epsilon_\infty^{2d}(\mathbf{k})}{2} \pm \frac{1}{2}\sqrt{[Z+\mu-\Sigma_\infty(Z)-\epsilon_\infty^{2d}(\mathbf{k})]^2-4t_\infty^2}. \tag{15}$$

The sign in Eq. (15) is chosen the same way as for Eq. (12). In our calculations, we also assume that the right function is equal to the value R_∞ found in the bulk, until we are within 30 planes of the first interface [for a ballistic-metal lead $\Sigma_\infty(Z)=0$]. Then we allow those 30 planes to be self-consistently determined with R_α possibly changing, and we include a similar 30 planes on the left-hand side of the last interface, terminating with the bulk result to the left as well.

Using the right and left functions, we finally obtain the Green's function

$$G_{\alpha\alpha}(\mathbf{k},Z)=\frac{1}{L_\alpha(\mathbf{k},Z)+R_\alpha(\mathbf{k},Z)-[Z+\mu-\Sigma_\alpha(Z)-\epsilon_\alpha^{2d}(\mathbf{k})]}, \tag{16}$$

where we used Eqs. (11) and (14) in Eq. (8). The local Green's function on each plane is then found by summing over the two-dimensional momenta, which can be replaced by an integral over the two-dimensional density of states (DOS),

$$G_{\alpha\alpha}(Z)=\int d\epsilon_\alpha^{2d}\,\rho^{2d}(\epsilon_\alpha^{2d})G_{\alpha\alpha}(\epsilon_\alpha^{2d},Z), \tag{17}$$

with

$$\rho^{2d}(\epsilon_\alpha^{2d})=\frac{1}{2\pi^2 t_\alpha^{\|}a^2}\mathbb{K}\left(1-\sqrt{1-\frac{(\epsilon_\alpha^{2d})^2}{(4t_\alpha^{\|})^2}}\right), \tag{18}$$

and $\mathbb{K}(x)$ the complete elliptic integral of the first kind. If $t_\alpha^{\|}$ varies in the nanostructure, then changing variables to $\epsilon=\epsilon_\alpha^{2d}/t_\alpha^{\|}$ in Eq. (17) produces

$$G_{\alpha\alpha}(Z)=\int_{-4}^{4}d\epsilon\frac{1}{2\pi^2a^2}\mathbb{K}\left(1-\sqrt{1-\frac{\epsilon^2}{16}}\right)G_{\alpha\alpha}(t_\alpha^{\|}\epsilon,Z), \tag{19}$$

so that we can take the ϵ variable to run from -4 to 4 for the integration on every plane, and we just need to introduce the corresponding $t_\alpha^{\|}\epsilon$ substitution (for ϵ_α^{2d}) into the left and right recurrence relations. In the bulk limit, where we use $t_\alpha=t$, we find that the local Green's function found from Eqs. (17) and (16) reduce to the well-known expressions for the three-dimensional Green's functions on a simple cubic lattice,[3] with a hopping parameter t.

Once we have the local Green's function on each plane, we can perform the DMFT calculation to determine the local self-energy on each plane.[9,10] We start with Dyson's equation, which defines the effective medium for each plane,

$$G_{0\alpha}^{-1}(Z)=G_\alpha^{-1}(Z)+\Sigma_\alpha(Z). \tag{20}$$

The local Green's function for the αth plane satisfies

$$G_\alpha(Z)=(1-w_1)\frac{1}{G_{0\alpha}^{-1}(Z)+\frac{1}{2}U}+w_1\frac{1}{G_{0\alpha}^{-1}(Z)-\frac{1}{2}U}, \tag{21}$$

with w_1 equal to the average filling of the localized particles [note that this above form is slightly different from the usual notation,[10] because we have made the theory particle-hole symmetric by the choice of the interaction in Eq. (1), so that $\mu=0$ corresponds to half-filling in the barrier region and in the ballistic metal leads]. Finally, the self-energy is found from

$$\Sigma_\alpha(Z)=G_{0\alpha}^{-1}(Z)-G_\alpha^{-1}(Z). \tag{22}$$

The full dynamical mean field theory algorithm can now be stated. We begin by (i) making a choice for the self-energy on each plane. Next, we (ii) use the left and right recurrences in Eqs. (11) and (14) along with the bulk values found in Eqs. (12) and (15) and a choice for the number of self-consistently determined planes within the metal leads (which we choose to be 30 to the left and the right of the barrier interfaces) to calculate the local Green's function at each plane in the self-consistent region from Eqs. (16) and (19). Once the local Green's function is known for each plane, we then (iii) extract the effective medium for each plane from Eq. (20), (iv) determine the new local Green's function from Eq. (21), and (v) calculate the new self-energy on each plane from Eq. (22). Then we iterate through steps (ii)–(v) until the calculations have converged.

For all of the calculations in this work, we will assume the hopping matrix is unchanged in the metallic leads and the barrier, so all $t_{\alpha\alpha\pm1}$ and all $t_\alpha^{\|}$ are equal to t, which we take as our energy unit. We also work at the particle-hole symmetric point of half-filling for the conduction electrons and the localized electrons. This yields $w_1=1/2$ and $\mu=0$.

There are a number of numerical details that need to be discussed in these computations. First, one should note that the recurrence relations in Eqs. (11) and (14) always preserve the imaginary part of R or L during the recursion. Hence the recursion is stable when R or L is complex. On the other hand, when they are real, we find that the large root is stable. Since this is the physical root, the recursion relations are always stable. Second, the integrand can have a number of singularities in it. When we calculate the Matsubara Green's functions, the only singularity comes from the logarithmic singularity in the two-dimensional DOS. We remove that singularity from the integration by using a midpoint rectangular integration scheme for $0.5<|\epsilon|<4$, and we change the variables for the region $|\epsilon|<0.5$ from ϵ to $x^3=\epsilon$, which is finite as $x\to0$, and which has a finite slope as $x\to0$; this allows a midpoint rectangular integration scheme for $|x|<(0.5)^{1/3}$ to accurately determine this second piece of the integral. When we calculate the real frequency Green's functions, we have the logarithmic singularity, but we also can have a square-root singularity at the αth plane in the denominator of the integrand when $\mathrm{Im}\,\Sigma_\alpha(\omega)=0$ and $|\omega+\mu-\mathrm{Re}\,\Sigma_\alpha(\omega)-\epsilon|=2$. We define $a=\omega+\mu-\mathrm{Re}\,\Sigma_\alpha(\omega)+2$ and $b=\omega+\mu-\mathrm{Re}\,\Sigma_\alpha(\omega)-2$. Then, if $a<-4$ or $b>4$, the only singularity lies at $\epsilon=0$ as before. When $b<-4$, but $-4<a<4$, then there is a singularity at $\epsilon=a$; when $a>4$, but $-4<b<4$, then there is a singularity at $\epsilon=b$; and when $-4<a$, $b<4$, there are singularities at a and b. The singularities are easy to transform away by using sine and hyperbolic cosine substitutions like $\epsilon=\omega+\mu-\mathrm{Re}\,\Sigma_\alpha(\omega)-2\sin\theta$ and $\epsilon=\omega+\mu-\mathrm{Re}\,\Sigma_\alpha(\omega)-2\cosh\theta$ into the respective pieces of the integrands where a singularity lies. We simply determine where all possible singularities lie (for each plane), set up an appropriate grid for the ϵ variable that takes the different changes of integration variable into account, and compute the associated weight functions for the integrations, in order to perform the integration over the two-dimensional DOS. Third, we find that when the correlations in the barrier are strong enough that we are in the Mott insulator for the bulk material, and the barrier is sufficiently thick, then the self-energy develops a sharp structure, where the real part goes through zero over a small range close to $\omega=0$, and the imaginary part picks up a large delta-function-like peak around $\omega=0$. In order to

properly pick up this behavior in the self-consistent solutions, we need to use a very fine integration grid (we used up to one million points for the calculations reported here) to perform the integration over the two-dimensional DOS. Such a fine grid is only needed for frequencies close to $\omega=0$, but one needs to have a fine enough frequency grid in ω to pick up the sharp peak behavior in the self-energy (we use a step size of 0.001 when there is a sharp structure in the self-energy). For ordinary ω points, we typically used an integration grid of 5000 points. Fourth, these equations are easy to parallelize on the real-frequency axis, because the calculations for each value of frequency are completely independent of one another, so we simply use a master-slave approach and send the calculations at different frequencies to each of the different slaves until all frequencies are calculated. This approach has an almost linear scale up in the parallelization speed.

In addition to these single-particle properties, we also are interested in transport along the z axis (perpendicular to the multilayered planes). The resistance of the nanostructures can be calculated by a Kubo-based linear response formalism[11] (i.e., a current-current correlation function). We begin with the current operator at the αth plane,

$$\mathbf{j}_z = \sum_\alpha \mathbf{j}_{z\alpha},$$

$$\mathbf{j}_{z\alpha} = \frac{ieat}{\hbar} \sum_{i \text{ in } 2d \text{ plane}} (c^\dagger_{\alpha i} c_{\alpha+1 i} - c^\dagger_{\alpha+1 i} c_{\alpha i}). \tag{23}$$

This operator sums all of the current flowing from the αth plane to the $\alpha+1$ plane.

The current-current correlation function is defined to be

$$\Pi_{\alpha\beta}(i\nu_l) = \int_0^\beta d\tau\, e^{i\nu_l\tau} \langle \mathcal{T}_\tau \mathbf{j}^\dagger_{z\alpha}(\tau) \mathbf{j}_{z\beta}(0)\rangle, \tag{24}$$

with $i\nu_l = i\pi T 2l$ the Bosonic Matsubara frequency and with the dc conductivity matrix determined by the analytic continuation of Eq. (24) to the real frequency axis via

$$\sigma_{\alpha\beta}(\nu) = \lim_{\nu\to 0} \mathrm{Re}\, \frac{i\hbar \Pi_{\alpha\beta}(\nu)}{\nu}. \tag{25}$$

In the spirit of the DMFT, we evaluate the two-particle correlation function in Eq. (24) by the bare bubble with no vertex corrections. In homogeneous systems in infinite dimensions, this procedure is exact, but it is only approximate for our inhomogeneous three-dimensional system (and even for inhomogeneous systems in infinite dimensions); nevertheless, we expect the corrections to be small. Substituting Eq. (23) into Eq. (24), evaluating the contractions in terms of the single-particle Green's functions, performing the integration over τ to convert to the Matsubara frequency representation, and performing a Fourier transform over the $2d$ spatial coordinates, yields the following result after some straightforward algebra:

$$\begin{aligned}\Pi_{\alpha\beta}(i\nu_l) = \left(\frac{eat}{\hbar}\right)^2 T\sum_m a^2 \sum_{\mathbf{k}} [& - G_{\beta+1\alpha+1}(\mathbf{k}, i\omega_m) \\ & \times G_{\alpha\beta}(\mathbf{k}, i\omega_m + i\nu_l) \\ & + G_{\beta\alpha+1}(\mathbf{k}, i\omega_m) G_{\alpha\beta+1}(\mathbf{k}, i\omega_m + i\nu_l) \\ & + G_{\beta+1\alpha}(\mathbf{k}, i\omega_m) G_{\alpha+1\beta}(\mathbf{k}, i\omega_m + i\nu_l) \\ & - G_{\beta\alpha}(\mathbf{k}, i\omega_m) G_{\alpha+1\beta+1}(\mathbf{k}, i\omega_m + i\nu_l)].\end{aligned} \tag{26}$$

Now we need to perform the analytic continuation from the imaginary to the real frequency axis.[12] This is done by first converting the summations over the Matsubara frequencies into contour integrals that enclose all of the Matsubara frequencies and are multiplied by the Fermi-Dirac distribution function $f(\omega)=1/[1+\exp(\beta\omega)]$ which has a pole at each Matsubara frequency. Then the contours are deformed to go along lines parallel (but just above or just below) the real axis, and the real axis shifted by $-i\nu_l$. At this point we replace $f(\omega - i\nu_l)$ by $f(\omega)$ and then analytically continue $i\nu_l \to \nu + i0^+$. The algebra is once again straightforward but somewhat tedious. The final result is

$$\begin{aligned}\Pi_{\alpha\beta}(\nu) = -\frac{1}{\pi}\left(\frac{eat}{\hbar}\right)^2 a^2 \sum_{\mathbf{k}} \{ & f(\omega)[G_{\alpha\beta}(\mathbf{k}, \omega+\nu)\mathrm{Im}\, G_{\beta+1\alpha+1}(\mathbf{k},\omega) + G_{\alpha\beta+1}(\mathbf{k},\omega+\nu)\mathrm{Im}\, G_{\beta\alpha+1}(\mathbf{k},\omega) + G_{\alpha+1\beta}(\mathbf{k},\omega+\nu) \\ & \times \mathrm{Im} G_{\beta+1\alpha}(\mathbf{k},\omega) - G_{\alpha+1\beta+1}(\mathbf{k},\omega+\nu)\mathrm{Im}\, G_{\beta\alpha}(\mathbf{k},\omega)] + f(\omega+\nu)[- G^*_{\beta+1\alpha+1}(\mathbf{k},\omega)\mathrm{Im}\, G_{\alpha\beta}(\mathbf{k},\omega+\nu) \\ & + G^*_{\beta\alpha+1}(\mathbf{k},\omega)\mathrm{Im}\, G_{\alpha\beta+1}(\mathbf{k},\omega+\nu) + G^*_{\beta+1\alpha}(\mathbf{k},\omega)\mathrm{Im}\, G_{\alpha+1\beta}(\mathbf{k},\omega+\nu) - G^*_{\beta\alpha}(\mathbf{k},\omega)\mathrm{Im}\, G_{\alpha+1\beta+1}(\mathbf{k},\omega+\nu)]\}.\end{aligned} \tag{27}$$

The last step is to evaluate the dc conductivity matrix, which becomes

$$\begin{aligned}\sigma_{\alpha\beta}(0) = \frac{2e^2}{h} a^4 t^2 \int d\epsilon\, \rho^{2d}(\epsilon) \int d\omega \left(-\frac{df}{d\omega}\right) [& \mathrm{Im}\, G_{\beta\alpha+1}(\epsilon,\omega)\mathrm{Im}\, G_{\alpha\beta+1}(\epsilon,\omega) + \mathrm{Im}\, G_{\beta+1\alpha}(\epsilon,\omega)\mathrm{Im}\, G_{\alpha+1\beta}(\epsilon,\omega) \\ & - \mathrm{Im}\, G_{\beta+1\alpha+1}(\epsilon,\omega)\mathrm{Im}\, G_{\alpha\beta}(\epsilon,\omega) + \mathrm{Im}\, G_{\beta\alpha}(\epsilon,\omega)\mathrm{Im}\, G_{\alpha+1\beta+1}(\epsilon,\omega)].\end{aligned} \tag{28}$$

The conductivity matrix has the dimensions e^2/ha^2, which is the inverse of the resistance unit, divided by two factors of length, and is the correct unit for the conductivity matrix (the mixed-basis Green's function $G_{\alpha\beta}$ has dimensions $1/ta^2$).

Since the conductivity matrix is not as familiar as the scalar conductivity used for homogeneous problems, we will briefly derive how one extracts the resistance of the nanostructure from the conductivity matrix. The key element that we use is that the current density that flows through each plane is conserved, because charge current can neither be created nor destroyed in our device. The continuity equation, then says that the current density through the αth plane, I_α, is related to the electric field, E_β, between the βth and $\beta+1$ plane via

$$I_\alpha = a\sum_\beta \sigma_{\alpha\beta}(0)E_\beta = I, \tag{29}$$

where we set the current density on each plane equal to a constant value I. Inverting this relation to determine the electric field gives

$$E_\beta = \frac{1}{a}\sum_\alpha [\sigma^{-1}(0)]_{\beta\alpha} I. \tag{30}$$

The voltage across the nanostructure is just the sum of the electric field between each plane, multiplied by the interplane distance (we assume a constant dielectric constant throughout), so we can immediately determine the resistance-area product (specific resistance) from Ohm's law

$$R_n a^2 = \frac{V}{I} = \sum_{\alpha\beta} [\sigma^{-1}(0)]_{\beta\alpha}. \tag{31}$$

One needs to pursue a similar type of analysis to examine the thermal transport properties (thermopower and thermal resistance), but it is somewhat more complicated, because the thermal current is not conserved from one plane to another plane, as is the charge current. We will present results for such a calculation elsewhere (at half-filling, where we restrict ourselves in this paper, there is no thermopower by particle-hole symmetry).

The only mathematical issue associated with this analysis is that we have assumed the conductivity matrix is invertible. In general, this is not true when there is no scattering in the metallic leads. In this case, we need to truncate the conductivity matrix to consider only the block that covers all of the planes in the barrier and the first metallic plane to the left and to the right of the barrier. This matrix is always invertible, and allows calculations to be performed easily (if we were to include a larger matrix, we find that the resistance does not increase as we increase the number of planes within the metallic leads that we include in the conductivity matrix block that is inverted, at least until we run into precision issues for the calculations). Of course, if the metallic leads have scattering, there are no numerical issues associated with the matrix inversion (except when the matrix is made too large and the system has approached the bulk limit, see below), but we need to decide how far down the metallic leads we will perform the actual measurement, since the voltage grows with the thickness of the metallic leads included in the calculation (when there is scattering in the leads).

In order to calculate the dc conductivity matrix in Eq. (28), we need to evaluate the off-diagonal components of the Green's functions. This is easy to do using the renormalized perturbation expansion, and the right and left functions. We find two recurrence relations

$$G_{\alpha\alpha-n}(\epsilon,\omega) = -\frac{G_{\alpha\alpha-n+1}t_{\alpha-n+1\alpha-n}}{L_{\alpha-n}(\epsilon,\omega)} \tag{32}$$

(defined for $n>0$) and

$$G_{\alpha\alpha+n}(\epsilon,\omega) = -\frac{G_{\alpha\alpha+n-1}t_{\alpha+n-1\alpha+n}}{R_{\alpha+n}(\epsilon,\omega)} \tag{33}$$

(also defined for $n>0$). The other off-diagonal Green's functions are found from the symmetry relations $G_{\alpha\alpha-n}=G_{\alpha-n\alpha}$ and $G_{\alpha\alpha+n}=G_{\alpha+n\alpha}$.

The computation of the junction resistance for a given temperature is relatively simple to perform. First, one must calculate all of the local self-energies for each plane, using the algorithm described above. Then, for each frequency ω, one can calculate all of the Green's functions that enter into the formula for $\sigma_{\alpha\beta}(0)$. It is best to evaluate the integral over ω for many different temperatures "at the same time" since the only thing that changes with temperature (when at half-filling, where the chemical potential is fixed and does not vary with T) is the Fermi factor derivative. Since evaluating at each frequency is independent of every other frequency, this algorithm is also "embarrassingly parallel."

One final comment is in order about the formalism for calculating the junction resistance. Namely, how does it relate to a Landauer approach to the resistance? In the Landauer approach[2] one does not calculate a conductivity matrix, but instead determines the transport directly by evaluating the Green's function $G_{\alpha\beta}$ where α lies at the left interface and β lies at the right interface. We believe one can show that these two approaches are completely equivalent if one uses the same self-energies for the inhomogeneous structure to calculate the Green's functions that enter into the transport calculation. We will examine this relationship in a future paper.

In a homogeneous (bulk) noninteracting system, we find that the Green's functions satisfy

$$G_{\alpha\alpha\pm n}(\epsilon,\omega) = \frac{-i}{\sqrt{4t^2-(\omega+\mu-\epsilon)^2}} \times \left[-\frac{\omega+\mu-\epsilon}{2} + i\frac{\sqrt{4t^2-(\omega+\mu-\epsilon)^2}}{2}\right]^n \tag{34}$$

when ϵ lies within the band $[|\omega+\mu-\epsilon|<2]$. Note that $\mathrm{Im}\, G_{\alpha\beta}(\epsilon,\omega)$ is not always negative when $\alpha\neq\beta$. This occurs because we are using a mixed basis, and the imaginary part of the Green's function does not have a definite sign in this basis. We can substitute these Green's functions into the expression for the conductivity matrix, to evaluate the result for the bulk. We find the matrix has all of its matrix elements equal to each other, and they assume the value

$$\sigma_{\alpha\beta}(0) = \frac{e^2}{ha^2}\int_{-2}^{2} d\epsilon\, \rho^{2d}(\epsilon) \approx 0.63\frac{e^2}{ha^2}, \qquad (35)$$

for the case of half-filling $\mu=0$ (since every matrix element is the same, the conductivity matrix is not invertible, but the resistance can still be calculated). This result will lead to precisely the Sharvin contact resistance[13–15] when we convert the conductivity into a resistance (the resistivity of a ballistic metal vanishes, but the resistance is nonzero).

III. SINGLE-PARTICLE PROPERTIES

We perform our calculations at half-filling ($\mu=0$, $\langle c_i^\dagger c_i\rangle = 1/2$, and $w_1=\langle w_i\rangle=1/2$). This has a number of advantages. First, because the chemical potential is the same for the metallic leads and the barrier, there is no electrochemical force that reorganizes the electrons to a screened dipole layer at each of the interfaces, instead the filling remains homogeneous throughout the system. Second, the chemical potential is fixed as a function of temperature, so there is no need to perform imaginary-axis calculations to determine the chemical potential as a function of temperature. We usually calculate the Matsubara Green's functions anyway, to test the accuracy of the real-axis Green's function, by comparing the Matsubara Green's functions calculated directly with those calculated from the spectral formula via the real-axis DOS (usually the accuracy is better than three decimal points for every Matsubara frequency). Third, we can perform calculations of the resistance at all temperatures in parallel, because the chemical potential does not vary with temperature (recall, the DOS of the Falicov-Kimball model is temperature independent for the DMFT solution[16]). Fourth, the particle-hole symmetry of the DOS allows us to have another check on the accuracy of the calculations because we do not invoke that symmetry in our calculations. Fifth, there is a metal-insulator transition (MIT) in the bulk Falicov-Kimball model on a cubic lattice when $U\approx 4.9t$, so the solutions at half-filling include the MIT. For these reasons, we find this case to be the simplest one to consider in a first approach to the inhomogeneous many-body problem.

We also reduce the number of parameters in our calculations by assuming all of the hopping matrix elements are equal to t for nearest neighbors. This is by no means necessary, but it allows us to reduce the number of parameters that we vary in our calculations, which allows us to focus on the physical properties with fewer calculations. The hopping scale t is used as our energy scale. We also include 30 self-consistent planes in the metallic leads to the left and to the right of our barrier, which is varied between 1 and 80 planes in our calculations.

The first problem we investigate is the extreme quantum limit of having one atomic plane in the barrier of our device. We tune the Falicov-Kimball interaction in the one barrier plane from $U=1$ to $U=20$, which goes from a dirty metal to well into the Mott insulating regime. But the Mott insulating phase does not like being confined to a single atomic plane, and there is a metallic proximity effect, where the metallic DOS leaks into the insulator DOS at low energies. The result is that we do not expect the single-plane barrier to be too resistive. This is easiest to see when we consider the local DOS within the barrier plane, as plotted in Fig. 1. There we see that the DOS starts to be reduced at the chemical potential as we increase U, but there is still substantial DOS at the Fermi energy when $U\approx 4.9$. In fact, as U is increased, we see that the upper and lower Mott-Hubbard bands form, centered at $\pm U/2$, but there is significant DOS that remains centered at $\omega=0$, and it even develops a small peak for $U>10$. The origin of, and the size of this peak, can be shown to arise naturally from the renormalized perturbation theory expressions for the Green's functions, but we do not do so here.[17] We anticipate that these states are localized at the interface, and represent the states that an incident electron can tunnel through to go from one metallic lead to the other in a transport experiment. These results show a number of interesting features of the coupling of a Mott insulator to a metallic lead: (i) the Mott transition remains in the sense that Mott-Hubbard bands continue to form, with their origin clearly seen near the MIT; (ii) the interface-localized states have a metallic character (i.e., a peak at $\omega=0$) in the large-U regime; and (iii) the proximity effect appears to always be active, and able to create states within the barrier at low energy, but the total weight in those states is low, so medium to high energy properties of the Mott insulator phase will remain similar to the bulk.

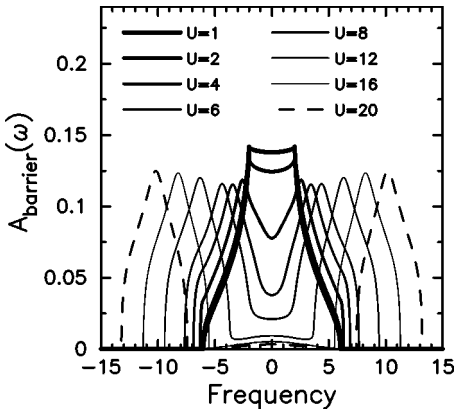

FIG. 1. Barrier DOS as a function of the Falicov-Kimball interaction U. The different line widths and styles denote different U values, as detailed in the legend. Note how the DOS initially evolves as in the bulk, with the DOS being reduced near $\omega=0$, and the bandwidth increasing. But as we pass through the Mott transition, we see that the double-peak Mott-Hubbard bands appear, but so does a low-energy (interface-localized) band near $\omega=0$, which looks like a low-weight metallic band for large U.

Next we examine what happens as we increase the barrier thickness for given values of U. Our focus is on three generic values of interest, $U=2$, which is a strongly scattering, diffusive metal; $U=4$, which is so close to the MIT, that the bulk DOS show a significant dip near $\omega=0$; and $U=6$, which is well within the Mott-insulating phase. We first examine how the metallic leads are influenced by the presence of the barrier. We set the origin of the α variables so that $\alpha=0$ corresponds to the first barrier plane (hence planes -1 to -30 represent the 30 planes to the left of the barrier, with -1 closest to the barrier). In Fig. 2, we show results for $U=2$ and five representative planes in the metal (the device has

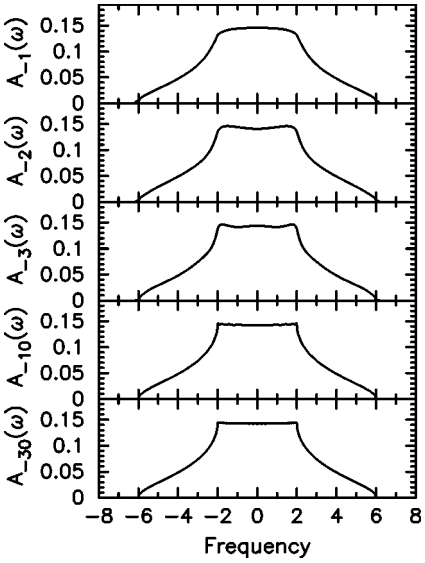

FIG. 2. Lead DOS for an $N=5$ barrier device with $U=2$. The different panels show the DOS in the first metal plane to the left of the barrier, in the second, the third, the tenth, and the thirtieth. Note how the system approaches the bulk cubic DOS as it moves further from the interface, as expected. A careful examination of the panels shows that the "flat" region with $|\omega|<2$ shows a half-period oscillation for each unit of distance from the current plane to the interface, but the amplitude shrinks dramatically as we move further from the interface.

five barrier planes). In Fig. 3, we show the same results for $U=4$ and in Fig. 4, we show the same results for $U=6$. The first thing to notice is that the DOS is close to that of the bulk simple cubic lattice for 30 planes away from the interface, indicating that our choice of 30 self-consistent planes is reasonable. Next, note that the amplitude of the oscillations grows as U increases. Third, the number of half periods in

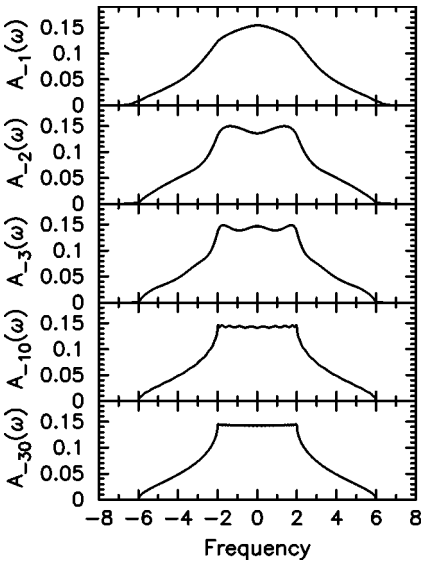

FIG. 3. Lead DOS for an $N=5$ barrier device with $U=4$. The different panels show the DOS in the first metal plane to the left of the barrier, in the second, the third, the tenth, and the thirtieth. Note how the amplitude of the oscillations increases as U increases.

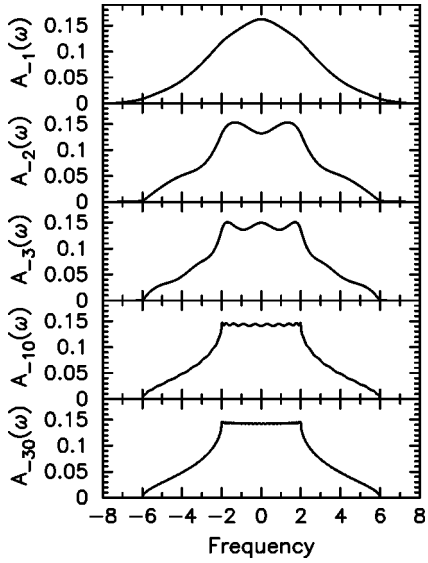

FIG. 4. Lead DOS for an $N=5$ barrier device with $U=6$. The different panels show the DOS in the first metal plane to the left of the barrier, in the second, the third, the tenth, and the thirtieth. Note how the amplitude of the oscillations is even larger here. A careful examination shows there are also oscillations (with the same kind of increase in the number of half periods with the distance from the interface) in the region $|\omega|>2$.

the oscillations increases with the distance away from the interface (both for $|\omega|<2$ and $|\omega|>2$). The source of these oscillations is the Friedel oscillations (with a wavelength on the order of two lattice spacings for half-filling) that we expect associated with the disturbance of the Fermi sea of the metal by the proximity to the interface.

There are two interesting questions to ask about these results: how thick does the barrier have to be before the Friedel oscillations become frozen in the metallic leads and do not change with a thicker barrier, and do we see oscillatory behavior in the barrier, where we instead expect there to be exponentially decaying wave functions? We find that the answer to the first question is that the structure is already essentially frozen in for a single-plane barrier, and it does not evolve much with the barrier thickness (although it does show evolution with the interaction strength). This perhaps sheds some light on why non-self-consistent Landauer based approaches for transport have been so successful. If one has a good guess for the semi-infinite lead DOS, then it does not change much as the thickness increases, so that guess will work well for all calculations with the same strength of electron correlations.

To examine the second question, we plot results for the DOS at a fixed frequency (four chosen for each U value) in Fig. 5. There are six different thicknesses plotted for each U value. The curves all lie on top of each other for the metallic lead planes, indicating that the Friedel oscillation structure is frozen in starting at $N=1$ (and we can read off the oscillation wavelength to be two lattice spacings, with a sharp decrease of the amplitude as one moves away from the interface). In the barrier, we see that there are only oscillations close to the interface, then the curves either flatten out or exponentially decay with thickness. But the curves continue to lie on top of

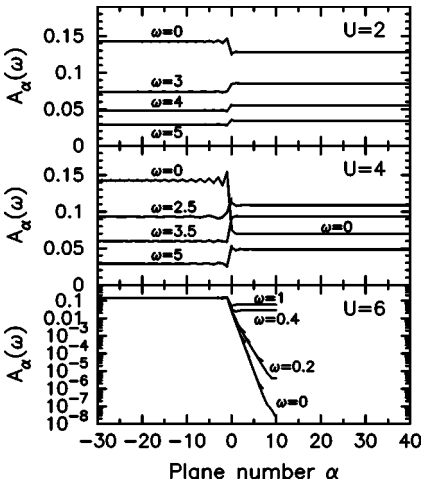

FIG. 5. DOS at specific values of ω as a function of the plane position in the device. We plot only the left-hand piece of the plots, since the right-hand piece is a mirror image of the left-hand piece. Note that the $U=6$ panel is a semilogarithmic plot. The four values of ω for $U=2$ are 0.0, 3.0, 4.0, and 5.0. The barrier thicknesses are $N=1$, 5, 10, 20, 40, and 80. The four values of ω for $U=4$ are 0.0, 2.5, 3.5, and 5.0. The barrier thicknesses are $N=1$, 5, 10, 20, 40, and 80. The four values of ω for $U=6$ are 0.0, 0.2, 0.4, and 1.0. The thicknesses are $N=1$, 4, 7, 10, 15, and 20. Note how all curves lie on top of each other in the metallic lead, indicating the structure in the metallic lead is frozen in for an $N=1$ barrier, and does not significantly change with increasing N. In the barrier, we only have oscillations at the interface, and then the curves either are flat with thickness ($U=2$ and 4), or exponentially decreasing or flat ($U=6$). The little tails that stick out for the lowest two frequencies with $U=6$ show that the middle plane of the barrier does not follow the same exponential decay as the other planes do. But the exponent of the exponential decay is frozen in starting at $N\approx 1$.

each other (except for the middle plane of the barrier for small ω and $U=6$). These results, once again, show that another of the assumptions of the non-self-consistent Landauer-based approaches, that there is an exponential decay with a well-defined decay length in the insulating barrier regions, holds here as well, but one needs to properly predict the decay length to perform accurate calculations.

Our final summary of the DOS is included in false color plots (the color, or gray scale, denoting the height of the DOS at a given plane) to emphasize the spatial location and amplitudes in the oscillations. Figure 6 shows the results for $N=1$ and $U=6$ and Fig. 7 shows the results with $N=20$ and $U=6$ (only one-half of the nanostructure planes are shown due to the mirror symmetry). The color scale (or gray scale) needs to use a banded rainbow, with the different colors (gray scales) separated by bands of black in order to pick up the small amplitude oscillations in the background of the large DOS. Note how the Friedel oscillations are essentially the same in the two plots, indicating this freezing of the oscillations starting at $N=1$. There are also oscillations visible near the metal band edges, indicating Friedel-type oscillations due to the different total bandwidths of the two materials joined in the nanostructure. The DOS in the barrier at low frequency becomes very small very quickly on these linear scales, but it is nonzero (see Fig. 5).

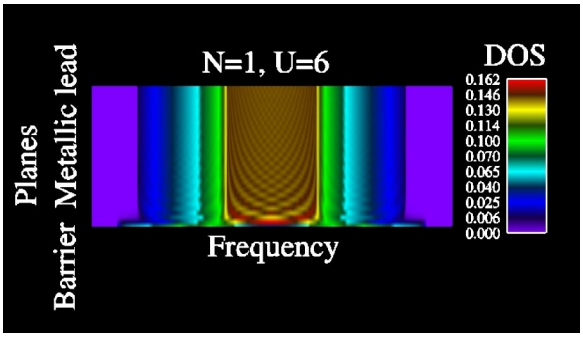

FIG. 6. (Color online) False-color plot of the DOS for a $N=1$ barrier plane device with $U=6$. The barrier plane is just the lowest plane at the bottom of the figure, while the 30 metallic planes lie on top. Note how the ripples of the Friedel oscillations are most visible in the central region, where the DOS has a plateau.

The final single-particle property we consider is the imaginary part of the self-energy at the central plane of the barrier at low energy in Fig. 8. In the bulk, the imaginary part of the self-energy vanishes within the Mott-Hubbard gap, except for a delta function at $\omega=0$ whose weight can be used as a quasiorder parameter for the Mott transition at half-filling (but not away from half-filling[18]). In the nanostructures, the imaginary part of the self-energy never vanishes in the bulk gap region, but it can assume very small values, with a sharp peak, of finite width, developing at $\omega=0$. This peak grows in height and narrows as the barrier is made thicker. It is a challenge to try to calculate such a structure numerically, especially due to the loss of precision in extracting the self-energy from the Dyson equation during the iterative algorithm. It requires a fine enough frequency grid to pick up the narrow structure, and it requires a sufficiently fine integration grid for ϵ, in order to accurately determine the peak value. Note how the self-energy evolves from a relatively broad featureless structure to a very sharply peaked structure as the barrier is made thicker. This kind of a peaked self-energy is similar to what is seen in the exact solution on the hypercubic lattice in infinite dimensions. There the Mott transition is actually to a pseudogap phase,

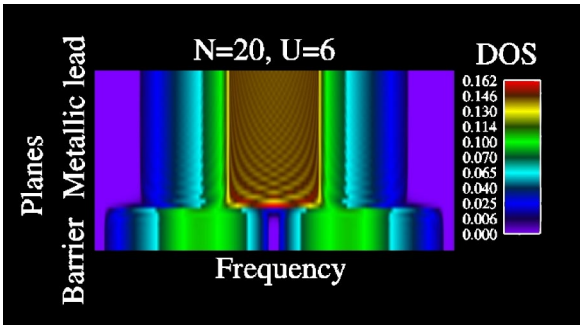

FIG. 7. (Color online) False-color plot of the DOS for a $N=20$ barrier plane device with $U=6$. The barrier planes are the lower 10 planes, while the 30 metallic planes lie on top. Note how the ripples of the Friedel oscillations agree with those in Fig. 6. In the barrier, the DOS decreases rapidly on this linear scale, and shows few oscillations, but one can see some small oscillations near the band edges in both regions.

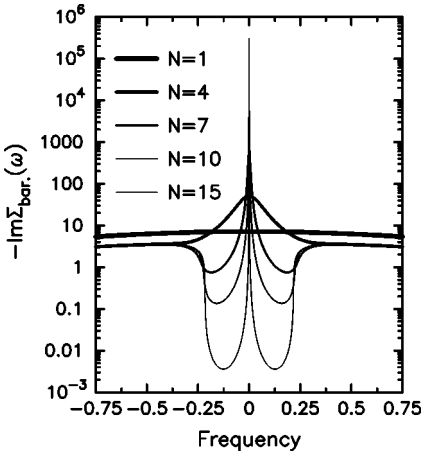

FIG. 8. Semilogarithmic plot of the imaginary part of the self-energy on the central plane of the barrier at small frequency for five different thickness barriers ($N=1$, 4, 7, 10, and 15). Note how the imaginary part of the self-energy becomes very small for frequencies close to $\omega=0$, but as we approach $\omega=0$, a sharp delta-function-like peak develops that narrows as the barrier is made thicker. It is precisely this structure that is hard to reproduce with numerical calculations. Note that this kind of a self-energy is very similar to what is seen in the hypercubic lattice in infinite dimensions.

with the DOS vanishing only at the chemical potential, but there is a region of exponentially small DOS in the "gap region." The sharp features in the self-energy led to a significant enhancement of the low-temperature thermopower on the hypercubic lattice when the system was doped off of half-filling[19] (and w_1 changed to produce an insulator). It is unclear at this point whether such behavior could lead to enhancements in the nanostructures, even though the self-energy has similar properties.

IV. GENERALIZED THOULESS ENERGY

It is important to try to bring semiclassical ideas of transport into transport in nanostructures, to see whether those concepts have useful quantum analogues. Thouless was the first to investigate such ideas for diffusive metal barriers.[4,5] He considered the idea of a dwell time in the barrier for an electron that tries to travel through the barrier. If we assume the electron takes a random walk through the barrier, then the time it spends inside the barrier is proportional to the square of the thickness of the barrier (with the proportionality being related to the diffusion constant). Since one can extract the diffusion constant, via an Einstein relation, from the junction resistance, Thouless could construct a quantum-mechanical energy $\hbar/t_{\mathrm{dwell}}$ from these classical ideas. It turns out that this energy scale plays a significant role in determining the quantum dynamics of many different kinds of nanostructures. For example, it can be easily generalized to take into account ballistic metals, where $t_{\mathrm{dwell}}=Na/v_F$ for a barrier of thickness Na, with v_F the Fermi velocity. The Thouless energy appears to be the critical quantum energy scale that determines the dynamics through weakly correlated nanostructures; its success in the theory of Josephson junctions is particularly noteworthy.[6]

So the fundamental question we wish to investigate is can the concept of a Thouless energy be generalized to a strongly correlated system, where transport through a nanostructure is either via tunneling or via incoherent thermal excitation. The answer is yes, and we do so by first trying to extract an energy scale from the resistance of the junction, which is able to track the putative thermal dependence of the resistance when we are in the incoherent thermal transport regime. A simple dimensionality argument shows that the form

$$E_{Th}=\frac{\hbar}{R_n a^2 2e^2\int d\omega[-df/d\omega]\rho_{\mathrm{bulk}}(\omega)Na} \tag{36}$$

has the kind of dependence we are looking for. The symbol $\rho_{\mathrm{bulk}}(\omega)$ is the local DOS in the bulk for the material that sits in the barrier of the nanostructure. If we check the dimensions, we see that R_n has dimensions h/e^2, and the DOS has dimensions $1/a^3t$, so E_{Th} is an energy [note Eq. (36) corrects typographical errors in an earlier work[7]]. When we examine systems where the barrier is a metal, then at low temperature the bulk DOS can be replaced by a constant in the integral, and we reproduce the known forms for the Thouless energy for ballistic ($E_{Th}\approx C/Na$) and diffusive ($E_{Th}\approx C'/[Na]^2$) electrons because the resistance is independent of the thickness for a ballistic metal barrier and it grows linearly with the thickness for a diffusive metal barrier. This method of generalizing the Thouless energy also avoids us having to try to answer the question of how long does it take an electron to tunnel from the left to the right lead, and it reproduces all of the known forms for the Thouless energy in a unifying formula that does not require us to even use the Einstein relation to extract a diffusion constant or to determine the Fermi velocity for an anisotropic Fermi surface (in the ballistic case).

We plot the results for this Thouless energy as a function of thickness in Fig. 9 for $U=4$. In panel (a), we multiply E_{Th} by the square of the length $L=Na$ of the barrier. The different curves correspond to different temperatures. If the Thouless energy went exactly like C'/L^2, then all of the curves would be straight lines, with a temperature-dependent value $C'(T)$. But we see some curvature for small barrier thicknesses. This arises mainly from the fact that in addition to the diffusive contribution to the resistance, there is a contact resistance, so for thin barriers, we do not have a pure $1/L^2$ behavior. Note, however, that the Thouless energy has little temperature dependence at low temperature, as expected. In panel (b), we plot the curves on a semilogarithmic plot, so one can see how small the Thouless energy becomes for thicker junctions.

The Thouless energy is plotted versus temperature on a log-log plot for $U=6$, which corresponds to a Mott-insulating barrier with a small correlation-induced gap. The dashed line indicates where $E_{Th}=T$, which is an important crossover point for dynamics, as we will see below. Note that the temperature dependence is significant in an insulator, because the integral in the denominator of Eq. (36) has strong temperature dependence in the insulator, but the resistance does not in the tunneling regime at low temperature. If we

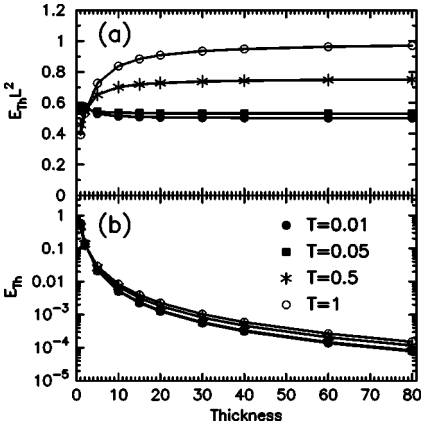

FIG. 9. Thouless energy for a $U=4$ (diffusive, but very strongly scattering metal) barrier as a function of the barrier thickness $L=Na$. The different curves correspond to different temperatures. The top panel multiplies the Thouless energy by L^2 to try to isolate the prefactor for the diffusive transport, while the bottom panel plots the Thouless energy on a semilogarithmic plot. Note that the temperature dependence of the constant, seen for thick barriers in panel (a), arises from the fact that the $U=4$ DOS has significant low-energy structure, because there is a dip that develops near the chemical potential, so the temperature dependence is both stronger than expected for normal metals, and anomalous because many more states are involved as T is increased, i.e., it behaves more like an insulator.

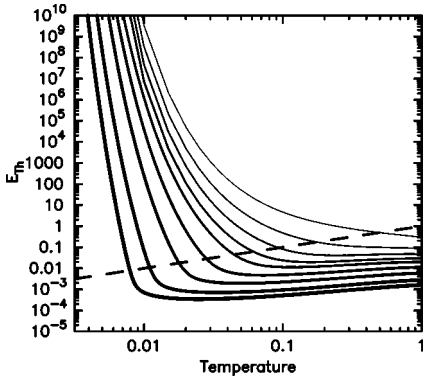

FIG. 10. Thouless energy for a $U=6$ (Mott-insulating) barrier as a function of temperature on a log-log plot. The different curves correspond to different thicknesses of the barrier, ranging from $N=1$ for the top curve to $N=2$, 3, 4, 5, 7, 10, 15, and 20 as we move down the plot. Note how the Thouless energy picks up dramatic temperature dependence here. The dashed line is the curve where $E_{Th}=T$. We find that when the Thouless energy equals the temperature, interesting effects occur (see below).

used the Thouless energy to determine the tunneling time via $t_{\text{tunnel}}=\hbar/E_{Th}$, we would find tunneling times rapidly approaching zero as $T\to 0$. We will not comment further here as to whether there is any substance to using such results to describe the quantum dynamics of the tunneling process. Instead we simply want to conclude that the concept of the Thouless energy can be generalized to strongly correlated systems, and we will see below that the crossover point where $E_{Th}\approx T$ has important physical interpretations that will be developed in the next section. Finally, the generalization of the Thouless energy to correlated systems changes the idea of a single energy scale being associated with the transport, since now the energy scale develops strong temperature dependence. If a single number is desired, then we would propose to use the energy scale where the Thouless energy is equal to the temperature, indicated by the points of intersection of the solid lines with the dashed curves in Fig. 10.

V. CHARGE TRANSPORT

The dc resistance is a low-energy property of the nanostructure, and so it requires the results of the single-particle properties to be determined accurately at low energy. This is not difficult for metallic barriers with any degree of scattering, as long as the numerical subtleties discussed above are taken into account in the analysis, but it does create problems for thick Mott insulators. We need to be able to properly determine the structure seen in Fig. 8 as the barrier is made thicker, and this can exhaust the numerical resources, or the numerical precision available for a given calculation. For our work, we were not successful in examining $U=6$ barriers thicker than $N=20$.

We plot the resistance-area product in Fig. 11 for $T=0.01$ and four different U values: $U=2$, a diffusive metal near the Ioffe-Regel limit of a mean free path on the order of a lattice spacing; $U=4$, a strongly scattering, anomalous metal, that has a strong dip in the DOS near the chemical potential; $U=5$, a Mott insulator that is nearly critical; and

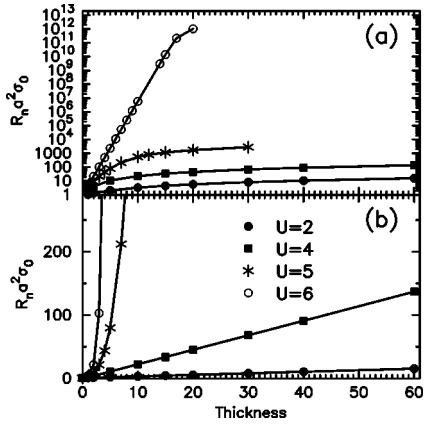

FIG. 11. Resistance-area product for nanostructures with $U=2$, 4, 5, and 6, and various thicknesses. Panel (a) is a semilogarithmic plot, while panel (b) is a linear plot. The temperature is $T=0.01$ in both panels. Note how the correlated insulator ($U=6$) has an exponential growth with thickness as expected for a tunneling process, but it turns over at the thickest junction, indicating a crossover to the incoherent transport regime. The $U=5$ data, which is close to the critical point for a MIT, has neither linear, nor exponential growth of its resistance-area product. The metallic cases ($U=2$ and 4) have perfect linear scaling of the resistance with current, with a nonzero intercept corresponding to the contact resistance. This may be surprising for $U=4$, because it is so strongly scattering (with a mean free path much less than a lattice spacing), that one would not think a semiclassical approach should apply there. The constant satisfies $\sigma_0=2e^2/ha^2$.

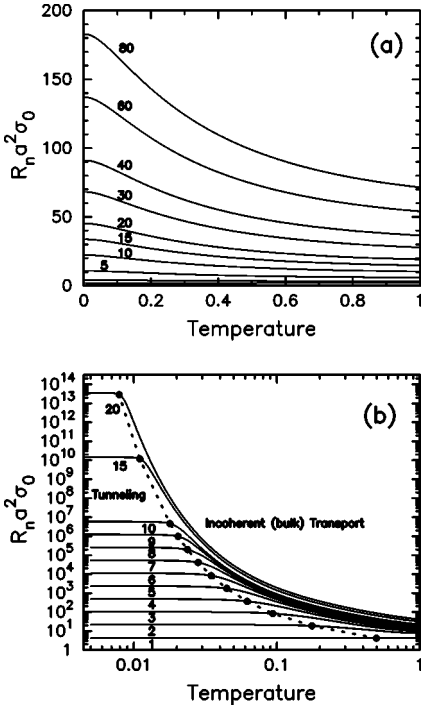

FIG. 12. Resistance-area product for nanostructures with (a) $U=4$ and (b) $U=6$ as a function of temperature [panel (a) is on a linear scale, and panel (b) is a log-log plot]. In panel (a) we include results for $N=1$, 2, (lowest two curves), 5, 10, 15, 20, 40, 60, and 80. Note how at each temperature there is a linear dependence of the resistance-area product with the thickness of the junction. Note further, that these junctions have anomalous temperature dependence for a metal (they actually look insulating in their dependence). In panel (b), we show the results for $U=6$ with $N=1-10$, 15, and 20. Note at low temperature we have tunneling, as the resistance-area product is weakly dependent on temperature, and the steps are equally spaced as a function of thickness, indicating exponential dependence on the thickness. At higher temperatures, there is a crossover to the incoherent transport regime, with the resistance-area product picking up a strong T dependence, and scaling linearly with the thickness. The dotted line that connects the solid dots is a plot of the resistance-area value at the temperature where $E_{Th}=T$ which determines the crossover.

$U=6$, a Mott insulator with a small correlation-induced gap. In panel (a), we have a semilogarithmic plot, which is useful for picking out tunneling behavior via an exponential increase of the resistance with thickness. This is clearly seen for the Mott insulator with $U=6$, with the beginnings of a crossover occurring near $N=20$, but the near-critical insulator at $U=5$ does not grow exponentially, nor does it grow linearly [see panel (b)]. The data for $U=2$ and $U=4$, both show linear increases with thickness, with a nonzero intercept on the y axis denoting the nonzero contact resistance with the metallic leads. It is surprising that this linear "ohmic" scaling holds for systems that are so strongly scattering, that their mean free path is much less than one lattice spacing.

Our final figure plots the resistance-area product versus temperature for (a) $U=4$ and (b) $U=6$ (Fig. 12). In panel (a), we can infer a linear dependence of $R_n a^2$ versus L for all temperatures, so this barrier is always ohmic in nature. But it has quite anomalous temperature dependence, looking like an insulator, whose resistance is reduced as the temperature increases. In panel (b), we see an exponential dependence of $R_n a^2$ versus L at low temperature, marked by the equidistant step increases of $R_n a^2$ as the thickness increases (recall this is a log-log plot). The temperature dependence is also weak in this region, indicated by the flatness of the curves. Hence the system is in the tunneling regime at low temperature. As T rises, there is a relatively sharp crossover region, where $R_n a^2$ begins to pick up strong (exponentially activated) T dependence, and $R_n a^2$ grows linearly with L. This is the incoherent "ohmic" regime for the transport. The solid dots represent the resistance-area product at the Thouless energy, determined by finding the temperature where $E_{Th}=T$ from Fig. 10, and marking those points on the curves in panel (b). A dashed line guide to the eye is drawn through these points. One can clearly see that the point where the Thouless energy equals the temperature determines the crossover from tunneling to incoherent transport. Surprisingly, this crossover occurs at a lower temperature for a thicker barrier. This occurs, because the tunneling resistance is higher for a thicker barrier. As T increases, the ohmic resistance, determined by multiplying the temperature-dependent bulk resistivity by the thickness and dividing by the area, will decrease. Once it is essentially equal to the tunneling resistance, there will be a crossover from tunneling, which provides a "quantum short" across the junction for low T, to "ohmic" (incoherent) thermally activated transport. This must occur at a lower temperature for more resistive junctions, and hence the thicker junctions have the crossover before the thinner junctions. Note that the temperature scale for this crossover does not appear to have any simple relation to the energy gap of the bulk material, instead it is intimately related to the dynamical information encoded in the generalized E_{Th} found in Eq. (36).

We do not consider thermal transport there, since the thermopower vanishes for this particle-hole symmetric case and the thermal resistance is not as interesting in systems with vanishing thermopower.

VI. CONCLUSIONS

In this contribution we worked with a generalization of DMFT to inhomogeneous systems to calculate the self-consistent many-body solutions for multilayered nanostructures that have barriers that can be tuned to go through the Mott transition. We developed the computational formalism thoroughly (based on the algorithm of Potthoff and Nolting), and although we applied it only to the Falicov-Kimball model, it is obvious that one can trivially add mean-field-like interactions such as Zeeman splitting for magnetic systems, or long-range Coulomb interactions for systems with mismatched chemical potentials. In addition, one can invoke whatever impurity solver desired for the local DMFT problem on each plane, which extracts a new self-energy from the current local Green's function. We studied both the single-particle properties and the charge transport.

There are a number of interesting results that came out of this analysis. First, we found that as the strength of the cor-

relations increases in the barrier, there is a stronger feedback effect on the Friedel-type oscillations that appear in the metallic leads, but those oscillations vary little with the thickness of the barrier for a fixed interaction strength. Second, there are few oscillations inside the barrier except close to the interface with the metallic leads, but the behavior in the barrier, of either an exponential decay, or of a constant DOS, gets frozen in for a relatively thin barrier, and the DOS changes little with increasing the thickness of the barrier, except when there is exponential decay which will always decrease within the correlation-induced gap. Third, the Mott insulating barrier develops a narrow peaklike structure in the imaginary part of the self-energy that approaches the bulk delta function result. This narrow and tall peak is difficult to determine accurately with the numerics and limits the ability to study thick insulating barriers. Fourth, we showed how to generalize the concept of a Thouless energy to become a function of T for a strongly correlated Mott insulator. Our unifying form for the Thouless energy includes the results for both the ballistic and diffusive metals as well. We identified an energy scale that describes the crossover from tunneling to incoherent transport in these nanostructures; it corresponds to $E_{Th}=T$. This energy scale is quite useful in other areas such as in the theory of Josephson junctions, which will be presented elsewhere. Sixth, we analyzed the resistance of these devices and found interesting behavior, including anomalous metallic behavior (but no tunneling) for a strongly scattering metal, and the crossover from tunneling to ohmic transport for insulating barriers.

This work also shed light on other approaches to transport through multilayered structures like the Landauer-based approaches. Usually these are non-self-consistent techniques that approach the problem from the point of view of transmission and reflection of Bloch waves moving through the device. We found that because the structure in the leads is frozen in beginning with $N=1$ and because the exponential decay lengths are also determined from $N=1$, if one knew those results and plugged them into the Landauer approach, one should be able to calculate accurate properties; i.e., the self-consistency is needed for each nanostructure, but the self-consistency hardly changes with the thickness of the barrier. Hence a phenomenological approach that adjusts the properties of the barrier height to produce the required behavior, may work well, even for strongly correlated systems; of course, the many-body theory is the only way to determine the precise structure needed via its self-consistent solution (i.e., it requires no fitting).

There are a number of important effects that we have not discussed here, which play roles in the transport through nanostructures. We did not attempt to include them in this first, simplest problem that we tackled. The first one is the issue of charge reorganization around the interface. If the chemical potentials of the leads and the barriers are different, electrons will spill from one plane to another until a screened dipole layer is formed, and a constant electrochemical potential is found throughout the device.[20] Such effects can have dramatic results if one or more of the materials is a correlated insulator, since the inhomogeneous doping of the system can transform part of it from insulating to metallic. This is believed to occur in grain boundaries in high temperature superconducting tapes and wires,[21] and in insulator-based nanostructures.[22,23] Second, calculations should be performed off of half-filling, where the thermal evolution of the chemical potential, will likely undergo some temperature dependence so the charge rearrangement can vary with temperature in the system. Third, we should calculate the thermal transport effects. Since these calculations require particle-hole asymmetry, we will have the chemical potential evolution and the charge reorganizations to deal with as well. Fourth, one can include ordered phase effects at the mean-field level easily, as in a superconductor for a Josephson junction,[24] or in a ferromagnet for a spintronics device. Fifth, it will be useful to determine the capacitance of a nanostructure, since the capacitance is often important in determining the switching speed of a device; it can be calculated with a linear-response formalism as well. Finally, we also should look into nonequilibrium effects, especially the nonlinear response of a current-voltage curve. It is our plan to investigate these complications in the future.

ACKNOWLEDGMENTS

The author would like to thank V. Zlatić for useful discussions. The author acknowledges support from the National Science Foundation under Grant No. DMR-0210717 and the Office of Naval Research under Grant No. N00014-99-1-0328. Supercomputer time was provided by the Arctic Region Supercomputer Center and by the Mississippi Region Supercomputer Center ERDC.

*Electronic address: freericks@physics.georgetown.edu; URL: http://www.physics.georgetown.edu/~jkf

[1] M. Potthoff and W. Nolting, Phys. Rev. B **59**, 2549 (1999).
[2] S. Datta, *Electronic Transport in Mesoscopic Systems* (Cambridge University Press, Cambridge, 1995).
[3] E. N. Economou, *Green's Functions in Quantum Physics* (Springer-Verlag, Berlin, 1983).
[4] J. T. Edwards and D. J. Thouless, J. Phys. C **5**, 807 (1972).
[5] J. D. Thouless, Phys. Rep., Phys. Lett. **13**, 93 (1974).
[6] P. Dubos, H. Courtois, B. Pannetier, F. K. Wilhelm, A. D. Zaikin, and G. Schön, Phys. Rev. B **63**, 064502 (2001).
[7] J. K. Freericks, Appl. Phys. Lett. **84**, 1383 (2004).
[8] L. M. Falicov and J. C. Kimball, Phys. Rev. Lett. **22**, 997 (1969).
[9] U. Brandt and C. Mielsch, Z. Phys. B: Condens. Matter **75**, 365 (1989).
[10] J. K. Freericks and V. Zlatić, Rev. Mod. Phys. **75**, 1333 (2003).
[11] R. Kubo, J. Phys. Soc. Jpn. **12**, 570 (1957).
[12] G. D. Mahan, *Many-Particle Physics* (Kluwer Academic, Berlin, 1990).
[13] Y. V. Sharvin, Zh. Eksp. Teor. Fiz. **48**, 984 (1965).

[14] Y. V. Sharvin, Sov. Phys. JETP **21**, 655 (1965).
[15] B. K. Nikolić, J. K. Freericks, and P. Miller, Phys. Rev. B **64**, 212507 (2001).
[16] P. G. J. van Dongen, Phys. Rev. B **45**, 2267 (1992).
[17] J. K. Freericks, cond-mat/0408225, Phys. Status Solidi B (to be published).
[18] D. O. Demchenko, A. V. Joura, and J. K. Freericks, Phys. Rev. Lett. **92**, 216401 (2004).
[19] J. K. Freericks, D. O. Demchenko, A. V. Joura, and V. Zlatić, Phys. Rev. B **68**, 195120 (2003).
[20] B. Nikolić, J. K. Freericks, and P. Miller, Phys. Rev. B **65**, 064529 (2002).
[21] H. Hilgenkamp and J. Mannhart, Rev. Mod. Phys. **74**, 485 (2002).
[22] A. Ohtomo, D. A. Muller, J. L. Grazul, and H. Y. Hwang, Nature (London) **419**, 378 (2002).
[23] S. Okamoto and A. J. Millis, Nature (London) **428**, 630 (2004).
[24] J. K. Freericks, B. K. Nikolić, and P. Miller, Int. J. Mod. Phys. B **16**, 531 (2002).